Pulse-front matching of ultrabroadband near-infrared noncollinear optical parametric amplified pulses

Oleksandr Isaienko and Eric Borguet*

Department of Chemistry, Temple University, 1913 N. 13th Street, Philadelphia, Pennsylvania 19122, USA
**Corresponding author: eborguet@temple.edu*

Received December 2, 2008; revised February 11, 2009; accepted February 16, 2009;
posted February 18, 2009 (Doc. ID 104724); published April 10, 2009

Noncollinear optical parametric amplifiers (NOPAs) pumped with ultrashort subpicosecond pulses often suffer from pulse-front tilting, resulting in angular dispersion and noncompressibility of the amplified signal pulses. We show that pulse-front matching (PFM) with a prism-telescope setup corrects for pulse-front tilts in a near-IR NOPA. We discuss the conditions that lead to pulse-front tilt and angular dispersion in NOPA-amplified signal pulses, thus requiring pulse-front mismatch correction. We review the method of PFM and describe the application of PFM to an 800 nm pumped near-IR NOPA based on a 2-mm-thick bulk potassium-titanyl phosphate (KTP) crystal. The introduction of pulse-front matching into the KTP-NOPA reduces the signal pulse angular dispersion significantly over the >35 THz bandwidth, thus nearly removing the pulse-front tilt. Compression of 1200 nm pulses to ~25 fs can be readily achieved with a fused-silica prism pair compressor.

OCIS codes: 190.4410, 190.4970, 190.7110, 320.7110.

1. INTRODUCTION

The generation of broadband ultrashort pulses in the near-infrared and midinfrared regions of the spectrum is important for applications such as high-harmonic generation and the production of attosecond pulses [1,2], ultrafast vibrational spectroscopy [3–6], optical network communications [7,8], and optical coherence tomography [9]. Noncollinear optical parametric amplifiers (noncollinear OPAs, NOPAs) have proven to be powerful tools for the generation of ultrabroadband and ultrashort pulses, traditionally in the visible range from blue-pumped β-BaB_2O_4 (BBO) NOPAs [10–13]. The noncollinear geometry allows the group velocities of signal and idler to be matched over a wide spectral range, leading to an order-of-magnitude increase in amplified bandwidths [14] compared to collinear OPA, where the group velocities of signal and idler pulses typically differ because of optical dispersion.

The method of NOPA has recently received increasing interest for the generation of broadband IR pulses. NOPA in bulk $KTiOAsO_4$ with 1050 nm pump was shown to generate high-power broadband pulses at ~1.5 μm [15,16]. Amplification of 1100–1300 nm signal pulses in 5-mm-thick $KTiPO_4$ (KTP) NOPA with bandwidths of ~50–60 nm was achieved [17]. A scheme has been proposedrequi for the extension of the principles of noncollinear optical parametric amplification into the near-IR part of the spectrum [18]. An experimental realization in a periodically poled stoichiometric $LiTaO_3$ resulted in the production of ultrabroadband pulses covering simultaneously the 1100–1600 nm wavelength region [18]. Compression of part of the pulse spectrum leads to nearly transform limited (TL) 16 fs pulses for those regions [18]. We have demonstrated the ability of bulk KTP to amplify broadband near-IR pulses covering simultaneously the spectral range of ~1050–1450 nm with a divergent seed beam [19].

With all its advantages for increasing the bandwidth of amplified pulses, the NOPA scheme, however, has a major drawback, especially pronounced when pumping with ultrashort (~0.1–1 ps) pulses. The physical length of ~100 fs pulses (either signal or pump) is on the order of tens of microns, which is often much less than the diameters of beams (hundreds of microns or even millimeters for high-energy amplifiers). Relatively large beam cross sections can cause spatiotemporal distortions of the signal pulses in the phase-matching plane. As a result, the amplified signal beam acquires a pulse-front tilt (Fig. 1) [20–24], i.e., a tilt of the front of the electric field envelope maxima with respect to the phase fronts (i.e., the fronts of electric field with same phase) (Fig. 2) which are normal to the beam direction of propagation [25,26]. Through the spatiotemporal coupling, different spectral components within the pulse spectrum travel at different angles, thus creating angular dispersion (Fig. 1) [21,24–29]. This phenomenon can be mathematically described if one takes into account variation in the phase of the electric field in the direction perpendicular to the beam propagation: $\varphi = \omega t - \mathbf{k}\cdot\mathbf{r} + \varphi_0 = \omega t - k_x \cdot x - k_z \cdot z + \varphi_0$ [25], where ω and t are the frequency and time, $\mathbf{r}$ is a radius vector, φ_0 is a constant initial phase, x and z are the coordinates normal to and along the beam propagation direction, $k_x = [2\pi n(\lambda)/\lambda]\sin(\varepsilon)$ and $k_z = [2\pi n(\lambda)/\lambda]\cos(\varepsilon)$ are the projections of the wave vector $\mathbf{k}$ onto the x and z axes, respectively, for each wavelength component propagating at some exit angle ε [Fig. 2(b)], and $n(\lambda)$ is the refractive in-

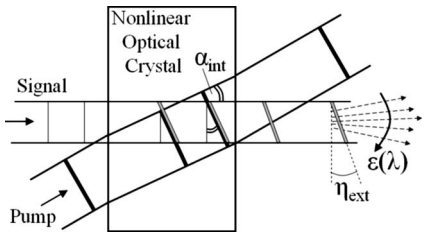

Fig. 1. Noncollinear geometry between femtosecond signal and pump beams induces a pulse-front tilt into signal pulses [24]. The pulse front of amplified signal pulses (gray bars) follows the pulse front of the pump pulses (black bars) resulting in the signal front tilted by angle α inside the nonlinear crystal (or η_{ext} after exiting the nonlinear crystal). The signal front tilt causes a nonzero angular dispersion $d\varepsilon/d\lambda$, where ε is the exit angle of a wavelength component λ.

dex of medium in which the tilted pulses propagate. Further, the pulse front can be mathematically described as a line in the xz coordinate system along which the phase does not vary with the frequency (Fig. 2) [25]: $d\varphi/d\omega = t - (dk_x/d\omega)\cdot x - (dk_z/d\omega)\cdot z = 0$. The slope of this line with respect to the x axis is equal to $-(dk_x/d\omega)/(dk_z/d\omega)$. On the other hand, because we chose the system of coordinates xz such that the x axis is parallel to the phase fronts, the slope of this line is $\tan\gamma$, where γ is the tilt angle of the pulse front [Fig. 2(b)]. After performing some algebraic transformations, one obtains the expression for the pulse-front tilt [25],

$$\tan\gamma = -\frac{n}{n-\lambda\dfrac{dn}{d\lambda}}\lambda\frac{d\varepsilon}{d\lambda} = -\frac{\nu_{group}}{\nu_{phase}}\lambda\frac{d\varepsilon}{d\lambda}, \qquad (1)$$

where $\nu_{phase}=c/n$ and $\nu_{group}=c/[n-\lambda(dn/d\lambda)]$ are the phase and group velocities of the electric field envelope, respectively. When the tilted pulses propagate in a low-dispersion medium (e.g., air), Eq. (1) can be simplified to $\tan\gamma=-\lambda(d\varepsilon/d\lambda)$ [25]. Equation (1) clearly demonstrates that if there is a nonzero pulse-front tilt angle γ, there will be a nonzero angular dispersion $d\varepsilon/d\lambda$.

This effect is very similar to passing a femtosecond beam through a prism, whereby the angular dispersion of the prism results in tilting of the pulse front [24,25,27]. The front tilt of the signal pulses makes it impossible to approach the TL duration because of the transversal chirp across the beam diameter [25–28]. Furthermore, it limits the minimum obtainable beam size [26,28], thus

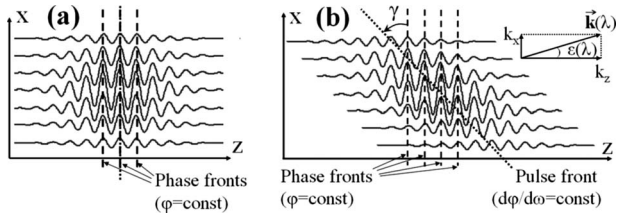

Fig. 2. Schematic representation of the electric field profile of an undistorted pulsed beam (a) and a beam with a pulse front tilted by angle γ (b). The x (z) axis is normal (along) the beam propagation direction. Phase fronts, as well as the pulse front in each case, are shown. $k=k(\lambda)$ is the wave vector corresponding to a frequency component $\omega=2\pi c/\lambda$, and $\varepsilon(\lambda)$ is the exit angle of the same frequency component (adapted from [26]).

leading to a decrease in the maximum available peak intensity of focused pulses [26,28]. Additionally, because of the angular dispersion all frequency components cannot be focused to a single spot [26].

According to Fig. 1, pulse-front tilting is a consequence of the large disproportion between the beam diameters and femtosecond pulse lengths. Correspondingly, the signal pulse-front tilt can be suppressed significantly if the pump and seed beam diameters at the nonlinear optical crystal are very small (thus approaching the physical length of pulses) and matched [30]. However, this approach is applicable only to low-energy NOPAs [30]. As an alternative, one can use pump pulses with durations long enough to fit the entire pulse front of the seed beam within the gain volume created by the pump pulses. This condition is practically met in high-energy optical parametric chirped-pulse amplifiers (OPCPAs) employing ~10–100 ps pump pulses, whereby the physical length of the pulses reaches several millimeters, or even up to a centimeter, comparable with the beam diameters used in these systems. The broadband seed pulses in such systems usually are generated from a femtosecond-oscillator laser, stretched ~1000 times, electronically synchronized with high-energy narrow band pump pulses from a Q-switched laser, and consecutively recompressed after amplification [31–38]. Noncollinearly amplified pulses from such OPCPAs were shown to be free of wave-front distortions and could be compressed very close to transform limit. However, if the seed and pump pulses are generated from the same laser, e.g., a femtosecond regenerative amplifier system, stretching of the pump pulses may not be applicable as it would lower the available peak intensities as well as require stretching the seed pulses (in order to suppress amplification of spontaneous emission) [39]. For high-energy ultrafast laser systems providing approximately millijoule pulses and above, it is desirable to have methods for correction of spatiotemporal distortions in femtosecond-pumped NOPAs. To our knowledge, neither pulse-front tilting nor its correction in a near-IR NOPA has been fully explored.

Here we demonstrate the possibility of precompensating for the signal pulse-front tilt in a near-IR NOPA pumped with ~100–200 fs, 800 nm pulses by introducing an appropriate tilt into the pump pulses, similar to the scheme employed in the visible pulse-front matched β-BaB_2O_4-based NOPA [21]. We apply this method to generate nearly pulse-front matched broadband ($\Delta\nu > 35$ THz) near-IR pulses from a bulk KTP NOPA and compare the results with the angular dispersion of the signal without tilting the pump pulse front. While the pulse spectrum supports ~16 fs pulses, compression to ~25 fs is demonstrated experimentally by using only a fused-silica prism pair compressor.

2. PULSE-FRONT MATCHING

In this section, we consider the theoretical basis for pulse-front tilting in a near-IR KTP-NOPA. First, we investigate the possibility of broadband NOPA in bulk KTP with a collimated seed beam in the near-IR range and perform calculations of the signal gain. Next, we review the connection between the angular dispersion of the non-pulse-

front matched signal beam and its pulse-front tilt. Finally, we review the method of pulse-front matching (PFM) with a prism-telescope setup and perform calculations for 800 nm pumped near-IR NOPA.

A. Phase Matching in KTP for Broadband Near-IR NOPA

Previously, we showed the possibility of broadband phase matching in bulk KTP in the near IR, if the white-light (WL) seed beam is focused in the crystal [19]: phase-matching curves corresponding to different noncollinear pump-seed angles can be simultaneously phase matched. However, even without a focused seed beam, relatively broadband phase matching is possible if the internal signal-pump noncollinear angle (α_{int}) is about 3°–4°. The signal gain profile for amplification of near-IR pulses was calculated for parameters close to experimental conditions using a plane-wave approximation with a nondepleted pump [14]. The results (Fig. 3) suggest that amplification of signal pulses with bandwidths as large as $\Delta\tilde{\nu} \sim 15$ THz is expected ($\sim 500\ \text{cm}^{-1}$ or $\Delta\lambda \sim 65$ nm at ~ 1150 nm) at noncollinear signal-pump angle $\alpha = 4.0°$ in 2-mm-thick KTP crystal when a collimated white-light seed beam is used.

B. Angular Dispersion and Pulse-Front Tilt of Signal Pulses from a Non-PFM-NOPA

As discussed above, one of the reasons for the distortions in the spatiotemporal profile of noncollinearly amplified signal pulses is a disproportion between the lengths of the interacting pulses and the beam diameters. These distortions can be suppressed if either the beam diameters are reduced close to physical lengths of pulses or the pulse width of pump is long enough to accommodate the entire signal pulse front. In the case of femtosecond-pumped NOPAs (especially, designed for high-energy outputs), the beam diameters can be several times larger than pulse lengths, and consequently when the fronts of the ultrashort pump and signal pulses are not parallel inside the nonlinear crystal, the front of the amplified signal pulses is tilted by the internal noncollinear angle α_{int} (Fig. 1). As a result, upon exiting the nonlinear crystal, the signal beam possesses an angular dispersion (spatial chirp) which, according to Eq. (1), is connected to the beam's pulse-front tilt angle through the following expression [22–25]:

$$\frac{d\varepsilon(\lambda)}{d\lambda} = -\frac{\tan\ \eta_{\text{ext}}}{\lambda_s}, \tag{2}$$

where $\varepsilon(\lambda)$ is the exit angle of a signal wavelength component λ, η_{ext} is the external pulse-front tilt angle of the signal pulses, and λ_s is the central signal wavelength. Additionally, because the group velocities of pulses inside the nonlinear crystal and in air significantly differ, so do the external and internal pulse-front tilts of the signal pulses. Using Eq. (1), one can derive the following expression for the connection between the external signal pulse-front tilt after exiting the nonlinear crystal and the internal pulse-front tilt η_{int} inside the crystal:

$$\tan\ \eta_{\text{int}} = \frac{\nu_s}{c}\tan\ \eta_{\text{ext}}, \tag{3}$$

where ν_s is the signal pulse group velocity in the nonlinear crystal. Thus, it is possible to estimate the tilt angle of the pulse front by measuring the angular dispersion of the pulses and, vice versa, it is possible to estimate the angular dispersion by knowing the front tilt angle.

C. Pulse-Front Matching with Front-Tilted Pump Pulses

Because relatively large-beam diameters (hundreds of microns or more) are used in high-power NOPAs, matching of pulse fronts of the pump and seed signal pulses inside the KTP crystal is needed [2,30,39]. In this work, we employ a prism-telescope setup in which the prism tilts the front of the pump pulses and the telescope images it to coincide with the front of the signal seed pulse (Fig. 4) [21].

In order to find a proper geometry for the prism-telescope setup, we use the following equations described in Refs. [22–24].

(i) The pulse-front tilt angle γ_{prism} of pump pulses incident onto a prism at an angle ϕ_1 right after the prism is defined by

$$\tan\ \gamma_{\text{prism}} = -\frac{\sin\ \theta_{\text{apex}}}{\cos\ \phi_1' \cos\ \phi_2}\lambda_p\frac{dn}{d\lambda_p}, \tag{4}$$

where θ_{apex} is the apex angle of the prism, n is the refractive index of the prism material, ϕ_1' is the angle of refraction, and ϕ_2 is the exit angle.

(ii) As the tilted pump pulses pass through a telescope with lenses of focal lengths f_1 and f_2, the pulse front is im-

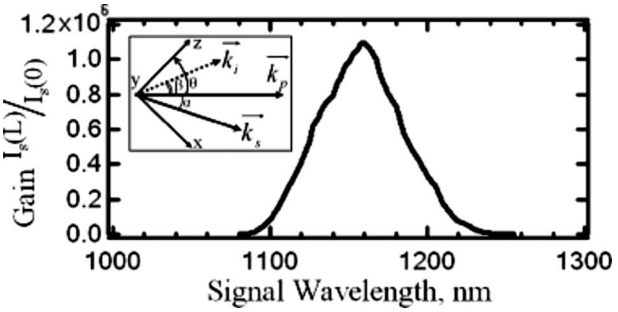

Fig. 3. Dependence of the signal gain coefficient on wavelength for the following parameters: crystal thickness $L = 2$ mm, $\lambda_{\text{pump}} = 800$ nm, pump pulse intensity $I_{\text{pump}} = 110\ \text{GW/cm}^2$, $\theta_{\text{pump}} = 48°$, and $d_{\text{eff}} = 2.955$ pm/V (type-II phase matching in xz plane [40,43]), $\alpha_{\text{int}} = 4°$. Inset: geometry of pump, signal, and idler beam wave vectors interacting inside the nonlinear optical crystal; the phase-matching angle, θ, between the pump wave vector and the z axis is defined, as well as the internal signal-pump noncollinear angle, α.

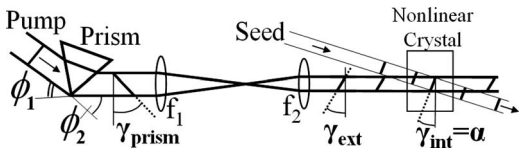

Fig. 4. Prism-telescope setup for pump-signal pulse-front matching [21]. γ_{prism} and γ_{ext} indicate the tilt angle of the 800 nm pulses after passing through the prism and the f_1/f_2 telescope, respectively. γ_{int} is the pump pulse-front tilt angle inside the nonlinear crystal, which is matched with signal-pump internal noncollinear angle α.

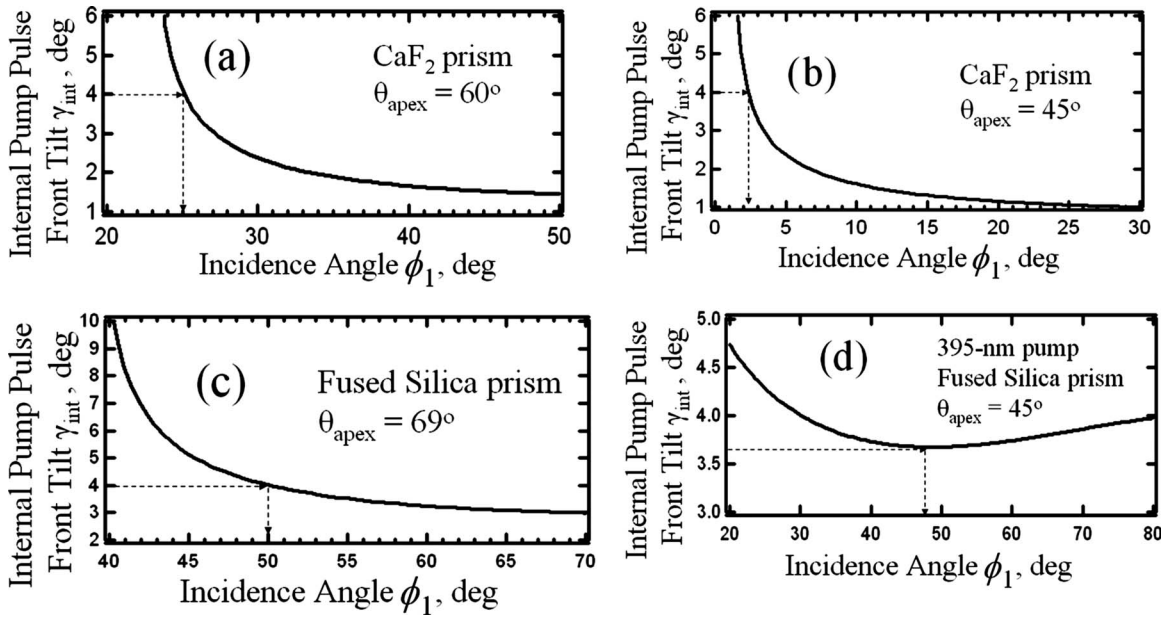

Fig. 5. Pulse-front tilt angle of the 800 nm pump pulses inside the KTP crystal induced by a CaF_2 prism with $\theta_{apex}=60°$ (a), a CaF_2 prism with $\theta_{apex}=45°$ (b), and a Brewster-angle fused-silica prism with $\theta_{apex}=69.0°$ and a 200–50 mm telescope, as a function of the incidence angle ϕ_1. (d) Pulse-front tilt angle of the 395 nm pump pulses as a function of the incidence angle ϕ_1 inside a BBO crystal calculated for the PFM-NOPA setup in [21].

aged with a longitudinal magnification factor f_1/f_2 so that the external pulse-front tilt at the nonlinear crystal is determined by

$$\tan\ \gamma_{ext} = \frac{f_1}{f_2}\tan\ \gamma_{prism}. \quad (5)$$

(iii) Finally, the refraction upon entering the nonlinear crystal reduces the pulse-front tilt by a factor of v_p/c (where v_p is the group velocity of pump in the nonlinear crystal), and so the internal pulse-front tilt is given by

$$\tan\ \gamma_{int} = \frac{v_p f_1}{c\ f_2}\tan\ \gamma_{prism}. \quad (6)$$

The proper parameters of the prism-telescope setup are found by stating the condition for pulse-front matching $\gamma_{int}=\alpha_{int}$. If the incidence of the pump pulse at the nonlinear crystal is not normal, there may be some deviations from Eq. (6). However, in practice, these deviations can be compensated by installing one of the lenses in the telescope onto a finely adjusted translation stage, thus the internal tilt of pump pulses can be tuned inside the crystal.

We carried out calculations of the internal pulse-front tilt angle γ_{int} as a function of the incidence angle ϕ_1 for the case of $f_1=200$ mm and $f_2=50$ mm (the focal lengths of the lenses used in the experiment) for each of the prisms available for this experiment: a CaF_2 prism with $\theta_{apex}=60°$ [Fig. 5(a)], a CaF_2 prism with $\theta_{apex}=45°$ [Fig. 5(b)], and a Brewster-angle fused-silica prism with $\theta_{apex}=69.0°$ [Fig. 5(c)]. The value of group velocity $v_p=c/1.8064$ for 800 nm *o*-polarized pulses in KTP was used [40]. For a comparison, we also calculated the dependence of γ_{int} on ϕ_1 for a fused-silica prism with $\theta_{apex}=45°$ for the case of PFM of visible signal pulses in a visible BBO-NOPA described in [21] ($f_1=200$ mm and $f_2=71$ mm, *e*-polarized 395 nm pump). As the calculations show, it is possible to create an internal pulse-front tilt in 800 nm pump pulses at an angle of ~4° with the 60°-apex angle CaF_2 prism [Fig. 5(a)] and the Brewster-angle fused-silica prism [Fig. 5(c)], although the curves at the desired value $\gamma_{int}=4°$ have a considerable slope, which requires an accurate adjustment of the ϕ_1 value. This is contrary to the convenient zero slope in the curve for the case of PFM in BBO-NOPA [21] [Fig. 5(d)], in which case the incident angle ϕ_1 need not be adjusted very precisely. Additionally, it can be seen that it would be practically challenging to adjust the incident angle if the 45°-apex angle CaF_2 prism is used [Fig. 5(b)] because of a relatively big slope at $\gamma_{int}=4°$. As the Brewster-angle fused-silica prisms were intended to be used for pulse compression, we decided to use the 60°-apex angle CaF_2 prism to tilt the pump pulse front. As can be seen from Eqs. (4)–(6), the internal pulse-front tilt of the pump is defined by the material of the tilting prism, its apex angle, and the focal lengths of the lenses in the telescope. The role of the material comes from the first derivative of the index of refraction vs wavelength. For example, at 800 nm for CaF_2 these values are approximately $-0.0105\ \mu m^{-1}$, $-0.0173\ \mu m^{-1}$ for fused silica, and $-0.0198\ \mu m^{-1}$ for BK7 [41]. Thus it is also possible that with a certain choice of the prism's material, apex angle, and telescope lenses, a curve similar to Fig. 5(d) can be obtained for 800 nm pulses with the flat bottom of the curve close to Brewster's angle.

3. EXPERIMENTAL SETUP

The experimental setup for the realization of a PFM KTP-NOPA is shown in Fig. 6. Briefly, the pump pulses at 800 nm (~803–804 nm in the actual current setup) are generated from a BMI-Coherent Alpha-1000 regenerative amplifier, as described elsewhere [42]. The pump pulses are ~150 fs long with energy of ~350 μJ and at a repeti-

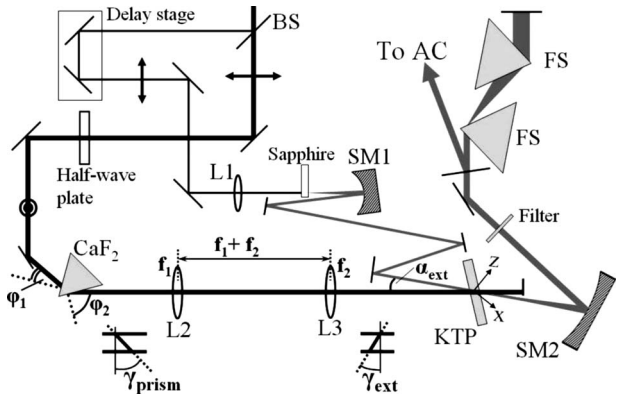

Fig. 6. Experimental setup of the pulse-front matched KTP-NOPA: BS, beam splitter; L, BK7 lenses; SM, spherical mirrors; CaF_2, equilateral prism (2.5 cm face size); sapphire, 2-mm-thick plate; KTP, 2-mm-thick crystal, cut at $\theta=42°$ for phase matching in xz plane (axes are shown); FS, Brewster-angle fused-silica prisms; and AC, autocorrelator. Double arrows and dotted circle indicate the polarization of 800 nm beam in and perpendicular to the plane of the drawing, respectively. γ_{prism} and γ_{ext} indicate the tilt angle of the 800 nm pulses after passing through the CaF_2 prism and the L2-L3 telescope, respectively.

tion rate of 1 kHz. The pulses are split into two parts: ~5–10 μJ is directed into the WL-seed generation arm and ~330–340 μJ is sent into the pump arm. The WL-seed pulses are generated at the very edge of a 2 mm sapphire plate and collimated with a silver spherical mirror with a minimal angle between incident and reflected beams to suppress the astigmatism (SM1, focal length of 2.5 cm). The 804 nm pulses in the pump arm are first passed through a half-wave plate (to make the pump o-polarized at the KTP crystal). After this, the front of pump pulses is tilted in an equilateral CaF_2 prism (face size of 2.5 cm). The pulse-front tilt was inverted with a telescope consisting of 200 mm and 50 mm lenses (L2 and L3 in Fig. 6, BK7) to match the pulse front of the WL signal seed inside the KTP crystal [21,22]. The 200 mm lens (L2 in Fig. 6) was mounted on a translation stage for fine adjustment of the lens position and, correspondingly, the tilt of the pump pulses inside the KTP crystal. The proper value of the pump incidence angle at a CaF_2-prism face ($\phi_1=25°$ in Fig. 6) was found by applying Eqs. (7)–(9) to the case of 800 nm centered pump and 200–50 mm lens telescope; the values of the index of refraction for CaF_2 and group velocity of the pump in KTP were taken from [41] and [40,43], respectively. At this value of ϕ_1, the internal tilt angle in pump pulses is expected to be ~4°. The WL seed and the pump beams were combined at the KTP crystal at an external noncollinear angle of $\alpha_{ext}\sim 7.0°$, corresponding to the internal noncollinear signal-pump angle $\alpha_{int}\sim 3.8°$. The incidence angle of the pump beam at the KTP crystal surface was set at ~9°, corresponding to the internal pump phase-matching angle $\theta\approx 47.1°$. The pump pulse energy at the KTP crystal was ~135 μJ, and the pump beam diameter at KTP was measured to be ~0.895 mm, resulting in the pump pulse intensity $I_p \approx 107$ GW/cm^2 (assuming ~200 fs pulse width). Energy losses were observed for the pump pulses after passing through the CaF_2 prism due to s-polarization at the prism faces, but in principle this can be corrected for by using p-polarized pump incident at Brewster's angle.

The optical setup without pulse-front tilting of the pump (Fig. 7) was essentially the same, except that instead of the CaF_2 prism there was a steering flat mirror and a pair of SF18 equilateral prisms oriented at Brewster's angle with respect to the pump beam (in this case, the half-wave plate was placed after the system of the prisms, so that the pump beam at the prism surfaces was p-polarized). This scheme provides for stretching of ~150 fs pump pulses to ~400–500 fs, ensures the time overlap between the WL-seed and pump pulses inside the KTP crystal, and is employed in our experiments on ultrabroadband KTP-NOPA with divergent seed [19]. We also verified that the two SF18 prisms at Brewster's angle do not induce a significant pulse-front tilt into the pump pulses. Spectra of the pump pulses were taken after passing through a 100-μm-wide slit as it was moved across the pump beam and corresponding center-of-mass wavelengths were calculated at corresponding exit angles (Fig. 7). The latter measurement shows that the center-of-mass wavelength varies only within 1 nm across the entire ~3 mm pump beam's cross section. The pump pulses were focused with a 300 mm lens (L4, Fig. 7) in such a way that the focal point was ~3–4 cm behind the KTP crystal [19]; thus the estimated pump beam diameter at the KTP crystal was ~300–400 μm to avoid damaging the crystal.

The signal beam after the KTP crystal was collimated with another spherical mirror (SM2, focal length of 200 mm). The amplified signal pulse spectra were acquired by measuring second-harmonic (SH) generation spectra of the signal beam off the surface of a 2-mm-thick polycrystalline ZnSe (P-ZnSe) crystal [44]. To determine the front tilt of signal pulses, the angular dispersion (or spatial chirp) of the amplified signal pulses was measured by moving a slit (100 μm width) across the signal beam and

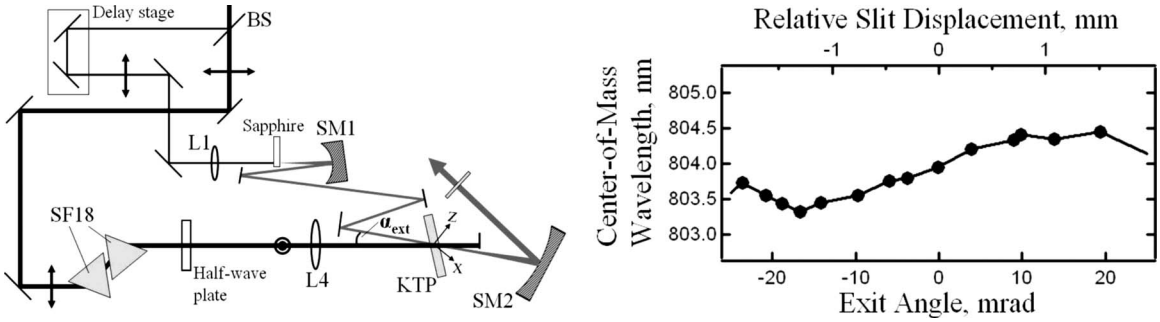

Fig. 7. Left: optical setup of KTP-NOPA without pulse-front matching: SF18, equilateral prisms; L4, BK7 lens. Right: angular dispersion of the pump pulses after passing through the two SF18 prisms (the solid line is a guide for the eyes).

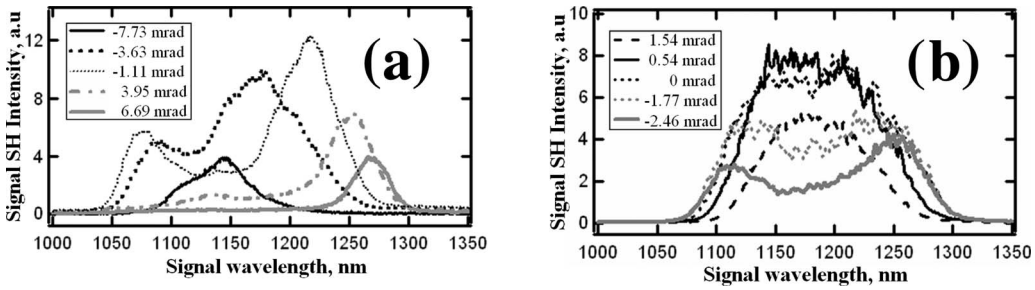

Fig. 8. Second-harmonic spectra of the signal pulses from the KTP-NOPA without (a) and with (b) pulse-front matching of the pump and seed pulses measured at different exit angles.

measuring signal SH spectra off the P-ZnSe crystal [21,24]. The amplified signal pulses from the PFM-NOPA were compressed in a Brewster-angle fused-silica-prism pair compressor and the pulse width was measured with a home-built autocorrelator using a 300-μm-thick BBO crystal.

4. RESULTS AND DISCUSSION

The angular dispersion of the amplified signal pulses in both nontilted pump and PFM configurations was measured by acquiring SH spectra of the signal as it was passed through the 100-μm-wide slit that was moved perpendicular to the beam direction. The values of the exit angle relative to the pump beam were calculated based on the slit displacement and its distance from the KTP crystal. Figure 8(a) shows the signal SH spectra at several values of the relative exit angle for nontilted pump configuration, while Fig. 8(b) shows the signal SH spectra measured the same way from the PFM configuration.

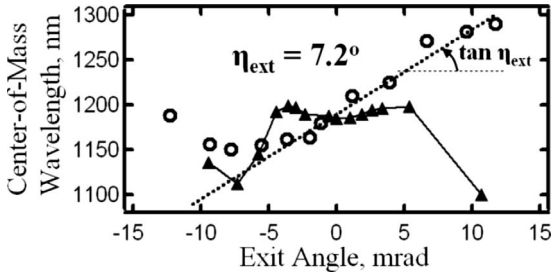

Fig. 9. Center-of-mass wavelengths of the signal pulses vs the exit angle for the non-PFM (open circles) and PFM (triangles) signal outputs; dashed line corresponds to the calculated angular dispersion of the signal pulses arising from noncollinear geometry between the seed and nontilted pump pulses for internal noncollinear angle $\alpha_{int}=\eta_{int}=4.0°$; Eqs. (2) and (3) were used. The solid line is a guide for the eyes.

Figure 9 shows the center-of-mass wavelengths of signal spectra at different exit angles [21] for both configurations. Also shown is the calculated external spatial chirp of the signal pulses from the nontilted configuration based on the internal noncollinear signal-pump angle of ~4° [dashed line; Eqs. (2) and (3) were used; value of the signal group velocity $\nu_s=c/1.819\ 61$ was applied [40]]. The experimental data for the spatial chirp of the signal pulses from the non-PFM NOPA geometry are in good agreement with expected angular dispersion, suggesting that this angular dispersion mostly results from the noncollinear geometry between the signal seed and the pump. It should be noted that even though the pump pulses were ~500 fs long in the non-PFM configuration, i.e., considerably longer than the initial ~150 fs pulses, the angular dispersion still was present in the amplified signal pulses. This was due to the fact that the physical length of pump pulses was still much shorter than the diameter of the pump beam. The PFM configuration generated signal pulses with nearly compensated angular dispersion and reduced output divergence. However, at certain values of exit angles, a separation of the signal spectra into two peaks at ~1100 and ~1300 nm was observed [Fig. 8(b)]. Taking into account the character of phase-matching curves in KTP [19], the latter can be related to the possibility of the white-light seed being not perfectly collimated.

The output signal pulse energy is ~4.5 μJ (photon conversion efficiency ≥4.5%). A typical spectrum of the signal pulses from the PFM-KTP-NOPA is shown in Fig. 10(a). For comparison, the normalized gain spectrum of signal pulses is shown on the same graph. The experimental

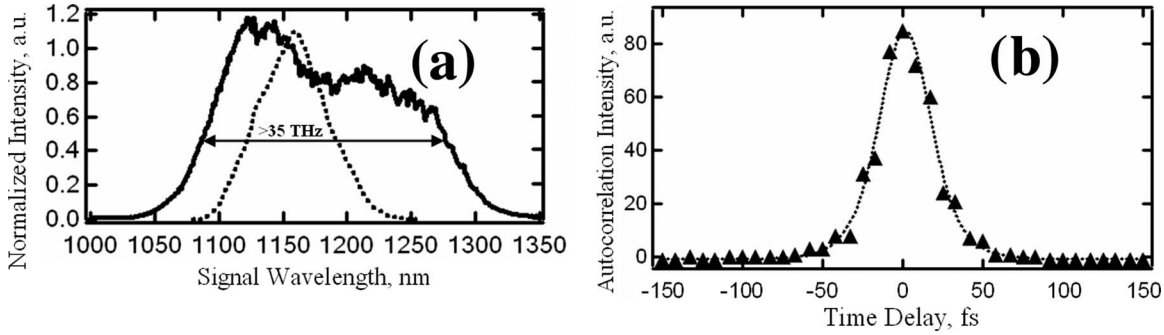

Fig. 10. (a) A typical SH spectrum of the amplified signal pulses from the PFM-NOPA (solid curve). For comparison, the gain spectrum from Fig. 3 is shown (dashed curve). (b) Autocorrelation of compressed signal pulses on a 300-μm-thick BBO crystal (triangles) and sech^2 fit (dotted curve).

bandwidth of signal pulses is larger than what is expected from the calculations. A possible reason for this may be some divergence of the seed beam at the KTP crystal.

Experimentally, the compression of the output pulses was carried out with a Brewster-angle cut fused-silica prism pair compressor. The interprism separation was 32.2 cm, corresponding to a net group delay dispersion (GDD) of −890 fs^2 [41,45–47]. This net GDD nearly compensates for the dispersion from the sapphire plate and the KTP crystal, as well as the initial ~150 fs duration of the 800 nm pulses. Figure 10(b) displays the autocorrelation of the compressed signal pulses acquired on a 300-μm-thick BBO crystal. The $sech^2$ fit of the autocorrelation yields ~25 fs pulse duration [full width at half maximum (FWHM) ~38.6 fs], while the transform limit (TL) pulse width for the spectrum in Fig. 10(a) is ~16 fs. The experimental pulse width is $\sim 1.6 \times$ TL, which may be a result of some uncompensated angular dispersion in the signal pulses [Fig. 8(b)]. Use of prisms with lower third-order dispersion (e.g., CaF_2 [18]) also may provide shorter near-IR pulses.

5. CONCLUSION

In conclusion, we have shown the generation of near-IR broadband pulses from a bulk KTP NOPA with nearly collimated WL seed. We have studied the effect of noncollinear geometry on the spatial properties of the near-IR NOPA signal output and characterized the pulse-front tilt of the signal pulses. We have applied the method of pulse-front matching to our near-IR KTP NOPA and produced ≥35 THz broad pulse-front tilt-free pulses centered at ~1200 nm. The fact that the bandwidth of nearly non-tilted amplified pulses is larger than what is expected from calculations for a collimated seed beam suggests that the method of PFM may be applied to NOPAs even when the seed beam has some divergence. We believe this method has also the potential for production of high-energy ultrabroadband near-IR pulses from a broad range of NOPAs employing other nonlinear crystals [18].

ACKNOWLEDGMENTS

The authors thank the Office of Basic Energy Sciences, U.S. Department of Energy (DOE) for financial support and acknowledge Professor Robert Stanley for lending the charge-coupled device (CCD) camera.

REFERENCES

1. J. Tate, T. Auguste, H. G. Muller, P. Salieres, P. Agostini, and L. F. DiMauro, "Scaling of wave-packet dynamics in an intense midinfrared field," Phys. Rev. Lett. **98**, 013901 (2007).
2. C. Vozzi, C. Manzoni, F. Calegari, E. Benedetti, G. Sansone, G. Cerullo, M. Nisoli, S. De Silvestri, and S. Stagira, "Characterization of a high-energy self-phase-stabilized near-infrared parametric source," J. Opt. Soc. Am. B **25**, B112–B117 (2008).
3. D. Polli, L. Luer, and G. Cerullo, "High-time-resolution pump-probe system with broadband detection for the study of time-domain vibrational dynamics," Rev. Sci. Instrum. **78**, 103108 (2007).
4. G. Cerullo, C. Manzoni, L. Luer, and D. Polli, "Time-resolved methods in biophysics. 4. Broadband pump-probe spectroscopy system with sub-20 fs temporal resolution for the study of energy transfer processes in photosynthesis," Photochem. Photobiol. Sci. **6**, 135–144 (2007).
5. S. Park, K. Kwak, and M. D. Fayer, "Ultrafast 2D-IR vibrational echo spectroscopy: a probe of molecular dynamics," Laser Phys. Lett. **4**, 704–718 (2007).
6. T. Kobayashi and Z. Wang, "Correlations of instantaneous transition energy and intensity of absorption peaks during molecular vibration: toward potential hyper-surface," New J. Phys. **10**, 065015 (2008).
7. Y. S. Seo, Y. Fujimoto, and M. Nakatsuka, "Optical amplification in a bismuth-doped silica glass at 1300 nm telecommunications window," Opt. Commun. **266**, 169–171 (2006).
8. O. Y. Jeon, M. J. Jin, H. H. Lim, B. J. Kim, and M. Cha, "Broadband optical parametric amplification at the communication band with periodically poled lithium niobate," Opt. Express **14**, 7210–7215 (2006).
9. D. Beitel, L. Carrion, L. R. Chen, and R. Maciejko, "Development of broadband sources based on semiconductor optical amplifiers and erbium-doped fiber amplifiers for optical coherence tomography," IEEE J. Sel. Top. Quantum Electron. **14**, 243–250 (2008).
10. T. Wilhelm, J. Piel, and E. Riedle, "Sub-20-fs pulses tunable across the visible from a blue-pumped single-pass noncollinear parametric converter," Opt. Lett. **22**, 1494–1496 (1997).
11. E. Riedle, M. Beutter, S. Lochbrunner, J. Piel, S. Schenkl, S. Sporlein, and W. Zinth, "Generation of 10 to 50 fs pulses tunable through all of the visible and the NIR," Appl. Phys. B **71**, 457–465 (2000).
12. A. Shirakawa and T. Kobayashi, "Noncollinearly phase-matched femtosecond optical parametric amplification with a 2000 cm^{-1} bandwidth," Appl. Phys. Lett. **72**, 147–149 (1998).
13. G. Cerullo, M. Nisoli, S. Stagira, and S. De Silvestri, "Sub-8-fs pulses from an ultrabroadband optical parametric amplifier in the visible," Opt. Lett. **23**, 1283–1285 (1998).
14. G. Cerullo and S. De Silvestri, "Ultrafast optical parametric amplifiers," Rev. Sci. Instrum. **74**, 1–18 (2003).
15. D. Kraemer, R. Hua, M. L. Cowan, K. Franjic, and R. J. D. Miller, "Ultrafast noncollinear optical parametric chirped pulse amplification in $KTiOAsO_4$," Opt. Lett. **31**, 981–983 (2006).
16. D. Kraemer, M. L. Cowan, R. Z. Hua, K. Franjic, and R. D. Miller, "High-power femtosecond infrared laser source based on noncollinear optical parametric chirped pulse amplification," J. Opt. Soc. Am. B **24**, 813–818 (2007).
17. H. K. Nienhuys and H. J. Bakker, "Noncollinear optical parametric amplification in potassium titanyl phosphate pumped at 800 nm," Appl. Opt. **47**, 2870–2873 (2008).
18. G. Cirmi, D. Brida, C. Manzoni, M. Marangoni, S. De Silvestri, and G. Cerullo, "Few-optical-cycle pulses in the near-infrared from a noncollinear optical parametric amplifier," Opt. Lett. **32**, 2396–2398 (2007).
19. O. Isaienko and E. Borguet, "Generation of ultra-broadband pulses in the near-IR by non-collinear optical parametric amplification in potassium titanyl phosphate," Opt. Express **16**, 3949–3954 (2008).
20. P. Di Trapani, A. Andreoni, C. Solcia, P. Foggi, R. Danielius, A. Dubietis, and A. Piskarskas, "Matching of group velocities in three-wave parametric interaction with femtosecond pulses and application to traveling-wave generators," J. Opt. Soc. Am. B **12**, 2237–2244 (1995).
21. A. Shirakawa, I. Sakane, and T. Kobayashi, "Pulse-front-matched optical parametric amplification for sub-10-fs pulse generation tunable in the visible and near infrared," Opt. Lett. **23**, 1292–1294 (1998).
22. T. Kobayashi and A. Shirakawa, "Tunable visible and near-infrared pulse generator in a 5 fs regime," Appl. Phys. B **70**, S239–S246 (2000).
23. T. Kobayashi and A. Baltuska, "Sub-5 fs pulse generation from a noncollinear optical parametric amplifier," Meas. Sci. Technol. **13**, 1671–1682 (2002).

24. T. Kobayashi, in *Femtosecond Optical Frequency Comb: Principle, Operation and Applications*, edited by J. Ye and S. T. Cundiff (Springer, Berlin, 2005), pp. 133–175.
25. J. Hebling, "Derivation of the pulse front tilt caused by angular dispersion," Opt. Quantum Electron. **28**, 1759–1763 (1996).
26. G. Pretzler, A. Kasper, and K. J. Witte, "Angular chirp and tilted light pulses in CPA lasers," Appl. Phys. B **70**, 1–9 (2000).
27. Z. Bor and B. Racz, "Group-velocity dispersion in prisms and its application to pulse-compression and traveling-wave excitation," Opt. Commun. **54**, 165–170 (1985).
28. K. Osvay, A. P. Kovacs, Z. Heiner, G. Kurdi, J. Klebniczki, and M. Csatari, "Angular dispersion and temporal change of femtosecond pulses from misaligned pulse compressors," IEEE J. Sel. Top. Quantum Electron. **10**, 213–220 (2004).
29. S. Akturk, X. Gu, E. Zeek, and R. Trebino, "Pulse-front tilt caused by spatial and temporal chirp," Opt. Express **12**, 4399–4410 (2004).
30. P. Tzankov, J. Zheng, M. Mero, D. Polli, C. Manzoni, and G. Cerullo, "300 μJ noncollinear optical parametric amplifier in the visible at 1 kHz repetition rate," Opt. Lett. **31**, 3629–3631 (2006).
31. C. P. Hauri, P. Schlup, G. Arisholm, J. Biegert, and U. Keller, "Phase-preserving chirped-pulse optical parametric amplification to 17.3 fs directly from a Ti: sapphire oscillator," Opt. Lett. **29**, 1369–1371 (2004).
32. N. Ishii, L. Turi, V. S. Yakovlev, T. Fuji, F. Krausz, A. Baltuska, R. Butkus, G. Veitas, V. Smilgevicius, R. Danielius, and A. Piskarskas, "Multimillijoule chirped parametric amplification of few-cycle pulses," Opt. Lett. **30**, 567–569 (2005).
33. S. Witte, R. T. Zinkstok, W. Hogervorst, and K. S. E. Eikema, "Generation of few-cycle terawatt light pulses using optical parametric chirped pulse amplification," Opt. Express **13**, 4903–4908 (2005).
34. S. Witte, R. T. Zinkstok, A. L. Wolf, W. Hogervorst, W. Ubachs, and K. S. E. Eikema, "A source of 2 terawatt, 2.7 cycle laser pulses based on noncollinear optical parametric chirped pulse amplification," Opt. Express **14**, 8168–8177 (2006).
35. F. Tavella, A. Marcinkevicius, and F. Krausz, "90 mJ parametric chirped pulse amplification of 10 fs pulses," Opt. Express **14**, 12822–12827 (2006).
36. F. Tavella, Y. Nomura, L. Veisz, V. Pervak, A. Marcinkevicius, and F. Krausz, "Dispersion management for a sub-10-fs, 10 TW optical parametric chirped-pulse amplifier," Opt. Lett. **32**, 2227–2229 (2007).
37. S. Adachi, H. Ishii, T. Kanai, N. Ishii, A. Kosuge, and S. Watanabe, "1.5 mJ, 6.4 fs parametric chirped-pulse amplification system at 1 kHz," Opt. Lett. **32**, 2487–2489 (2007).
38. S. Adachi, N. Ishii, T. Kanai, A. Kosuge, J. Itatani, Y. Kobayashi, D. Yoshitomi, K. Torizuka, and S. Watanabe, "5-fs, multi-mJ, CEP-locked parametric chirped-pulse amplifier pumped by a 450-nm source at 1 kHz," Opt. Express **16**, 14341–14352 (2008).
39. J. A. Fulop, Z. Major, A. Henig, S. Kruber, R. Weingartner, T. Clausnitzer, E. B. Kley, A. Tunnermann, V. Pervak, A. Apolonski, J. Osterhoff, R. Horlein, F. Krausz, and S. Karsch, "Short-pulse optical parametric chirped-pulse amplification for the generation of high-power few-cycle pulses," New J. Phys. **9**, 438 (2007).
40. A. Smith, "SNLO software package," http://www.as-photonics.com/?q=SNLO.
41. W. J. Tropf, M. E. Thomas, and T. J. Harris, in *Handbook of Optics*, edited by M. Bass (McGraw-Hill, New York, 1995), pp. 33.3–33.83.
42. D. Bodlaki and E. Borguet, "Picosecond infrared optical parametric amplifier for nonlinear interface spectroscopy," Rev. Sci. Instrum. **71**, 4050–4056 (2000).
43. V. G. Dmitriev, G. G. Gurzadyan, and D. N. Nikogosyan, *Handbook of Nonlinear Optical Crystals* (Springer, Berlin, 1999).
44. T. D. Chinh, W. Seibt, and K. Siegbahn, "Dot patterns from second-harmonic and sum-frequency generation in polycrystalline ZnSe," J. Appl. Phys. **90**, 2612–2614 (2001).
45. R. L. Fork, O. E. Martinez, and J. P. Gordon, "Negative dispersion using pairs of prisms," Opt. Lett. **9**, 150–152 (1984).
46. O. E. Martinez, J. P. Gordon, and R. L. Fork, "Negative group-velocity dispersion using refraction," J. Opt. Soc. Am. A Opt. Image Sci. Vis **1**, 1003–1006 (1984).
47. "Newport Corporation, Application Note 29: Prism Compressor for Ultrashort Laser Pulses," http://www.newport.com/file_store/Optics_and_Mechanics/AppsNote29.pdf.